

Self-induced transparency modelocking of quantum cascade lasers in the presence of saturable nonlinearity and group velocity dispersion

Muhammad Anisuzzaman Talukder and Curtis R. Menyuk

*Department of Computer Science and Electrical Engineering,
University of Maryland Baltimore County
1000 Hilltop Circle, Baltimore, MD 21250
anisuzzaman@umbc.edu*

Abstract: We consider the impact of saturable nonlinearity and group velocity dispersion on self-induced transparency (SIT) modelocking of quantum cascade lasers (QCLs). We find that self-induced transparency modelocking in QCLs can be obtained in the presence of saturable nonlinearity if the saturable loss or gain is below a critical limit. The limit for the saturable loss is significantly more stringent than the limit for the saturable gain. Stable modelocked pulses are also obtained in the presence of both normal and anomalous group velocity dispersion when its magnitude is below a critical value. The stability limit for the saturable loss becomes less stringent when group velocity dispersion is simultaneously present. However, the stability limit for the saturable gain is not significantly affected. All these limits depend on the ratio of the SIT-induced gain and absorption to the linear loss. Realistic values for both the saturable nonlinearity and chromatic dispersion are within the range in which SIT modelocking is predicted to be stable.

© 2010 Optical Society of America

OCIS codes: (140.5965) Semiconductor lasers, quantum cascade; (140.4050) Mode-locked lasers.

References and links

1. J. Faist, F. Capasso, D. Sivco, C. Sirtori, A. Hutchinson, and A. Cho, "Quantum cascade laser," *Science* **264**, 553–556 (1994).
2. C. Y. Wang, L. Kuznetsova, V. M. Gkortsas, L. Diehl, F. X. Kärtner, M. A. Belkin, A. Belyanin, X. Li, D. Ham, H. Schneider, P. Grant, C. Y. Song, S. Haffouz, Z. R. Wasilewski, H. C. Liu, and F. Capasso, "Mode-locked pulses from mid-infrared quantum cascade lasers," *Opt. Express* **17**, 12929–12943 (2009).
3. C. Y. Wang, L. Diehl, A. Gordon, C. Jirauschek, F. X. Kärtner, A. Belyanin, D. Bour, S. Corzine, G. Höfler, M. Troccoli, J. Faist, and F. Capasso, "Coherent instabilities in a semiconductor laser with fast gain recovery," *Phys. Rev. A* **75**, 031802 (2007).
4. C. Sirtori and R. Teissier, "Quantum Cascade Lasers: Overview of Basic Principles of Operation and State of the Art," in *Intersubband Transitions in Quantum Structures*, R. Paiella, ed. (McGraw-Hill, New York, 2006).
5. H. Choi, L. Diehl, Z.-K. Wu, M. Giovannini, J. Faist, F. Capasso, and T. B. Norris, "Gain recovery dynamics and photon-driven transport in quantum cascade lasers," *Phys. Rev. Lett.* **100**, 167401 (2008).
6. H. Choi, L. Diehl, Z.-K. Wu, M. Giovannini, J. Faist, F. Capasso, and T. B. Norris, "Time-resolved investigations of electronic transport dynamics in quantum cascade lasers based on diagonal lasing transition," *IEEE J. Quantum Electron.* **45**, 307–321 (2009).

7. H. Risken and K. Nummedal, "Self-pulsing in lasers," J. Appl. Phys. **39**, 4662–4672 (1968); R. Graham and H. Haken, "Quantum theory of light propagation in a fluctuating laser-active medium," Z. Phys. **213**, 420–450 (1968).
8. P. W. Smith, "The self-pulsing laser oscillator," IEEE J. Quantum Electron. **3**, 627–635 (1967).
9. T. Uchida and A. Ueki, "Self locking of gas lasers," IEEE J. Quantum Electron. **3**, 17–30 (1967).
10. H. A. Haus, "Theory of mode locking with a fast saturable absorber," J. Appl. Phys. **46**, 3049–3058 (1975).
11. S. L. McCall and E. L. Hahn, "Self-induced transparency by pulsed coherent light," Phys. Rev. Lett. **18**, 908–912 (1967).
12. S. L. McCall and E. L. Hahn, "Self-induced transparency," Phys. Rev. **183**, 457–489 (1969).
13. V. V. Kozlov, "Self-induced transparency soliton laser via coherent mode locking," Phys. Rev. A **56**, 1607–1612 (1997).
14. V. V. Kozlov, "Self-induced transparency soliton laser," JETP Lett. **69**, 906–911 (1999) [Pis'ma Zh. Eksp. Teor. Fiz. **69**, 856 (1999)].
15. C. R. Menyuk and M. A. Talukder, "Self-induced transparency modelocking of quantum cascade lasers," Phys. Rev. Lett. **102**, 023903 (2009).
16. M. A. Talukder and C. R. Menyuk, "Analytical and computational study of self-induced transparency modelocking in quantum cascade lasers," Phys. Rev. A **79**, 063841 (2009).
17. M. A. Talukder and C. R. Menyuk, "Effects of backward propagating waves and lumped mirror losses on self-induced transparency modelocking in quantum cascade lasers," Appl. Phys. Lett. **95**, 071109 (2009).
18. R. Paiella, F. Capasso, C. Gmachl, D. L. Sivco, J. N. Baillargeon, A. L. Hutchinson, A. Y. Cho, and H. C. Liu, "Self-mode-locking of quantum cascade lasers with giant ultrafast optical nonlinearities," Science **290**, 1739–1742 (2000).
19. A. Gordon, C. Y. Wang, L. Diehl, F. X. Kärtner, A. Belyanin, D. Bour, S. Corzine, G. Höfler, H. C. Liu, H. Schneider, T. Maier, M. Troccoli, J. Faist, and F. Capasso, "Multimode regimes in quantum cascade lasers: From coherent instabilities to spatial hole burning," Phys. Rev. A **77**, 053804 (2008).
20. H. Choi, L. Diehl, F. Capasso, D. Bour, S. Corzine, J. Zhu, G. Höfler, and T. B. Norris, "Time-domain upconversion measurements of group-velocity dispersion in quantum cascade lasers," Opt. Express **15**, 15898 (2007).
21. H. A. Haus, "Mode-locking of lasers," IEEE J. Sel. Quantum. Electron. **6**, 1173–1185 (2000).
22. L. Allen and J. H. Eberley, *Optical Resonance and Two Level Atoms* (Dover, New York, 1987).
23. R. W. Boyd, *Nonlinear Optics*, 2nd ed. (Academic Press, London, 2003).

1. Introduction

Modelocking of quantum cascade lasers (QCLs) [1] is an active field of research. They are the most useful semiconductor sources that operate in the mid-IR, and modelocking these lasers opens a path to generating short pulses in the mid-IR from a semiconductor source. That in turn has a host of military, communications, medical, and environmental sensing applications. While the generation of 3 ps pulses has been achieved using active modelocking [2], it has proved difficult to generate sub-ps pulses from QCLs using conventional modelocking because of the inherently narrow linewidth and short gain recovery time T_1 compared to direct-bandgap semiconductor lasers [3]. The linewidth in QCLs is narrow compared to direct-bandgap semiconductor lasers because the lasing transition takes place between two subbands within the conduction band [4]. The subbands have approximately the same curvature, so that the transition frequency only has a weak dependence on the electron temperature. The gain recovery time of a conventional QCL is generally on the order of a ps due to very fast carrier transport by resonant tunneling and LO phonon relaxation [5, 6], while the round-trip time T_{rt} in a typical 3-mm-long cavity of conventional QCLs is around 50 ps. The condition $T_1 \ll T_{rt}$ makes it difficult to form a pulse, and the laser may become unstable when operated above its threshold due to the Risken-Nummedal-Graham-Haken instability [7].

Though the fast gain recovery time and the narrow linewidth of the conventional QCLs are not suitable for conventional passive modelocking [8–10], these conditions are ideal for using the self-induced transparency (SIT) effect [11–14]. The relatively narrow linewidth compared to direct-bandgap semiconductor lasers corresponds to a relatively large coherence time T_2 , and the short recovery time implies that inversion in the gain medium will be restored during one round-trip of a short pulse. Recently, it has been theoretically demonstrated that QCLs can be modelocked using the SIT effect in their typical parameter range and that pulses on

the order of the coherence time T_2 can be generated [15–17]. For this purpose, QCLs must be grown with interleaved absorbing and gain periods. The absorbing periods stabilize the short pulses by absorbing continuous waves and shape the pulses as they propagate. These absorbing periods operate in a way that is analogous to a saturable absorber in a conventional passively modelocked laser.

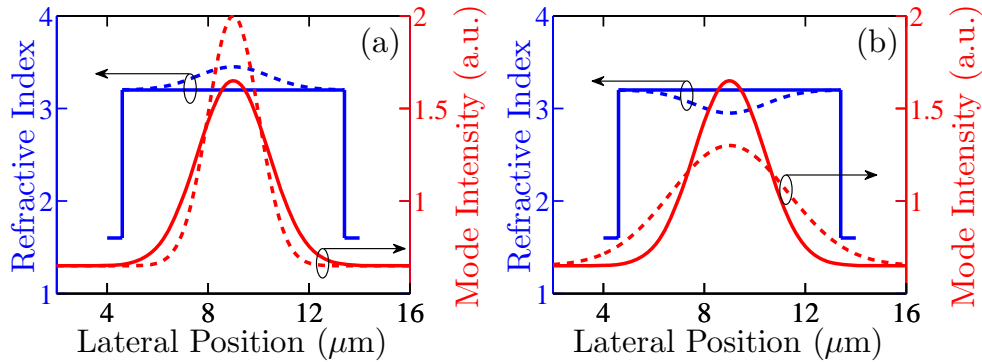


Fig. 1. Refractive index profile and resulting intensity distribution of the fundamental waveguide mode along the lateral direction of a conventional QCL waveguide in case of (a) saturable loss and (b) saturable gain. The intensity profile changes due to the strong index nonlinearity of the active region. (a) If the intensity increases, the index near the center of the waveguide increases and the mode is more tightly confined. (b) If the intensity decreases, the index near the center of the waveguide decreases and the mode is more weakly confined.

Paiella *et al.* [18] observed self-focusing due to a strong intensity-dependent refractive index in QCLs. In addition, Wang *et al.* [3] and Gordon *et al.* [19] found evidence for an intensity-dependent loss in QCLs. They found that the loss saturates when QCLs are operated with an input current that is above threshold. As the intensity of the light inside the laser increases, the intensity-dependent portion of the refractive index, n_2 , adds to the intensity-independent portion of the refractive index, n_0 . The total refractive index of the core increases. Therefore, the overlap of the lateral optical mode with the core increases, and the overlap with the lossy cladding decreases, as schematically shown in Fig. 1(a). As a result, the loss decreases. In practice, the change of the refractive index with intensity can be positive or negative, depending on the wavelength. When the sign of n_2 is negative, then the loss will increase because the overlap of the lateral optical mode with the lossy cladding will increase, as schematically shown in Fig. 1(b). Therefore, an optical pulse may experience saturable loss or saturable gain, depending on the wavelength of the laser transition.

Chromatic dispersion is also present in QCLs. Choi *et al.* [20] found for a particular QCL a dispersion coefficient $\beta_2 \sim -4.6 \text{ ps}^2/\text{m}$ at the $5 \mu\text{m}$ gain transition. Therefore, a pulse may broaden during propagation inside the laser structure.

Work to date on SIT modelocking of QCLs has not considered the intensity dependence of the refractive index when the pulse propagates in the laser structure or chromatic dispersion. In work to date, we have demonstrated analytically that SIT modelocking is possible under ideal conditions [15], and we have shown computationally that the modelocking is robust when the parameters of the Maxwell-Bloch equations vary from their ideal values [16]. We have also shown that SIT modelocking is robust when the geometric effects of bi-directional propagation and lumped mirror losses are considered [17]. Since the stability of SIT modelocking depends on the magnitude of the gain and absorption coefficients relative to loss, the modulation of

loss by the intensity will affect the stability of the SIT modelocking. Since SIT modelocking generates, in principle, pulses on the order of only 100 fs, chromatic dispersion, which spreads the pulses will also affect the stability. Therefore, it is critical to investigate the effects of the saturable nonlinearity and chromatic dispersion in order to determine the practicality of SIT modelocking.

In this work, we find that SIT modelocking is achieved in the presence of the saturable loss or the saturable gain, but only when the saturable loss and the saturable gain are below critical values. The limiting values of the saturable loss are significantly lower in magnitude than the limiting values of the saturable gain. The intensity and duration of the modelocked pulse depend on the amount of the saturable loss or saturable gain, in addition to the gain and absorption coefficients.

SIT modelocking is stable when the group velocity dispersion is normal or anomalous, in contrast to conventional passively modelocked systems that can be modeled by the complex Ginzburg-Landau equation [21]. In fact, as we will show, the pulse intensity as a function of time is the same regardless of the sign of the chromatic dispersion in SIT modelocking. The pulse intensity decreases and the pulse duration increases when the absolute value of the dispersion coefficient increases. Beyond a critical value that depends on the magnitude of the gain and absorption coefficients, the pulses become unstable. They either break up into multiple pulses due to the growth of continuous waves, or they damp away.

When saturable nonlinearity and group velocity dispersion are simultaneously present, as would be expected to occur in practice, the stability limit for the saturable loss increases, becoming less stringent, while the stability limit for the saturable gain remains almost unchanged. We will show that realistic values for the saturable nonlinearity and chromatic dispersion are within the range where SIT modelocked pulses are expected to be stable.

In this work, we do not consider the backward-propagating waves, which may interfere with the forward-propagating waves and create spatial hole burning. In Ref. 17, we showed that spatial hole burning is not an issue for SIT modelocking as long as continuous waves are suppressed, and continuous waves are always suppressed when SIT modelocking is stable.

In this work, we also do not consider the lumped mirror loss. The inclusion of the lumped mirror loss in the model does not change the results qualitatively, although there is some quantitative change [17]. The impact of the lumped mirror loss depends significantly on the cavity length. Quantum cascade lasers are generally 1–3 mm long. The impact of the lumped mirror loss on SIT modelocking will decrease as the cavity length increases. In order to focus on the effects of chromatic dispersion and saturable nonlinearity, we have added the mirror loss to the loss in the medium and distributed the total loss along the length of the cavity. However, if lumped mirror loss is included in the model, the realistic values for the saturable nonlinearity and group velocity dispersion will still be within the range where SIT modelocked pulses are expected to be stable. In Ref. 17, we found that due to lumped mirror loss, pulses decay with a smaller absorption coefficient for a given gain coefficient. Therefore, saturable loss, which sets the most stringent limits, will compensate the lumped mirror loss. The stability limits will increase, and SIT modelocking will be obtained with greater saturable loss.

The remainder of this paper is organized as follows: Sec. 2 presents the theoretical model of the pulse dynamics in QCLs that have interleaved gain and absorbing periods when saturable nonlinearity and group velocity dispersion are present. In Sec. 3, we show the effect of saturable loss or saturable gain on SIT modelocking. In Sec. 4, we show the effect of group velocity dispersion on SIT modelocking. In Sec. 5, we show the effect on SIT modelocking when both the saturable nonlinearity and group velocity dispersion are simultaneously present. Finally, in Sec. 6, we summarize the results and draw conclusions.

2. Theoretical model

We use the two-level approximation of the Maxwell-Bloch equations [22,23] to model the gain dynamics of a QCL. In SIT-modelocked QCL structures, the absorbing periods are interleaved with the gain periods. So, in the presence of saturable nonlinearity and group velocity dispersion, the Maxwell-Bloch equations can be written as

$$\frac{n}{c} \frac{\partial E}{\partial t} = -\frac{\partial E}{\partial z} - i \frac{kN_g \Gamma_g \mu_g}{2\epsilon_0 n^2} \eta_g - i \frac{kN_a \Gamma_a \mu_a}{2\epsilon_0 n^2} \eta_a - \frac{1}{2} l(|E|^2) E - i \frac{1}{2} \beta_2 \frac{\partial^2 E}{\partial t^2}, \quad (1.a)$$

$$\frac{\partial \eta_g}{\partial t} = \frac{i\mu_g}{2\hbar} \Delta_g E - \frac{\eta_g}{T_{2g}}, \quad (1.b)$$

$$\frac{\partial \Delta_g}{\partial t} = \frac{i\mu_g}{\hbar} \eta_g E^* - \frac{i\mu_g}{\hbar} \eta_g^* E + \frac{\Delta_{g0} - \Delta_g}{T_{1g}}, \quad (1.c)$$

$$\frac{\partial \eta_a}{\partial t} = \frac{i\mu_a}{2\hbar} \Delta_a E - \frac{\eta_a}{T_{2a}}, \quad (1.d)$$

$$\frac{\partial \Delta_a}{\partial t} = \frac{i\mu_a}{\hbar} \eta_a E^* - \frac{i\mu_a}{\hbar} \eta_a^* E + \frac{\Delta_{a0} - \Delta_a}{T_{1a}}, \quad (1.e)$$

where the subscripts g and a in Eq. (1) refer to the gain and absorbing periods, respectively. The independent variables z and t denote length along the light-propagation axis of the QCL and time. The dependent variables E , η_g , Δ_g , η_a , and Δ_a denote the envelope of the electric field, the polarization and inversion in the gain medium, and the polarization and inversion in the absorbing medium. The parameters Δ_{g0} and Δ_{a0} denote the equilibrium inversion away from the modelocked pulse. The parameters μ_g and μ_a denote the dipole moments. The parameters N and Γ denote the electron density and the mode overlap factor. The parameters n , c , k , ϵ_0 , and \hbar denote the index of refraction, the speed of light, the wavenumber in the active region, the vacuum dielectric permittivity, and Planck's constant. The parameter β_2 is the dispersion coefficient. The parameter $l(|E|^2)$ denotes the loss that depends on the light intensity.

Equation (1) is the same as in [16] except that here we include the effect of chromatic dispersion, and we allow $l(|E|^2)$ to depend on the field intensity. We may write the intensity-dependent loss as [21]

$$l(|E|^2) = l_0 - \gamma |E|^2, \quad (2)$$

where l_0 is the linear loss and γ is the saturable nonlinearity coefficient. According to Eq. (2), the loss will saturate when $\gamma > 0$ and the gain will saturate when $\gamma < 0$. The sign of γ depends directly on the sign of n_2 , which in turn depends on the wavelength of the laser transition [23]. Gordon *et al.* [19] found that γ depends sensitively on the width of the QCL active region. As the width of the active region increases, the parameter γ decreases. Gordon *et al.* found that γ decreases approximately by a factor of two when the width of the active region increases from 3 μm to 7.5 μm .

The performance and the stability of the SIT modelocking of QCLs depend on the gain and absorption coefficients from the gain and absorbing periods, respectively. The gain per unit length (g) and the absorption per unit length (a) are given by [16]

$$g = \frac{kN_g \Gamma_g \mu_g^2 T_{2g}}{2\epsilon_0 n^2 \hbar}, \quad a = \frac{kN_a \Gamma_a \mu_a^2 T_{2a}}{2\epsilon_0 n^2 \hbar}. \quad (3)$$

The stability of SIT modelocking does not depend on the absolute values of the gain and absorption coefficients, but rather on their values relative to the loss in the system. Therefore, it is useful to normalize the gain and absorption coefficients relative to the linear loss, i.e., $\bar{g} = g/l_0$ and $\bar{a} = a/l_0$. In this work, we have set $T_{2g} = T_{2a} = 100$ fs and $T_{1g} = T_{1a} = 1$ ps. We have set

$l_0 = 10 \text{ cm}^{-1}$ and $L_c = 3 \text{ mm}$. All these values are realistic [19]. We set $\mu_g/e = 1.8 \text{ nm}$, which corresponds to the design value that we reported in [16]. We also assume that the gain periods are completely inverted in equilibrium, i.e., $\Delta_{g0} = 1$, while the absorbing periods are completely uninverted in equilibrium, i.e., $\Delta_{a0} = -1$. The absorbing periods have a dipole moment twice as large as the dipole moment in the gain periods, i.e., $\mu_a/\mu_g = 2$. We have previously determined the impact of varying this ideal set of parameters, and we have found that SIT modelocking is robust over a wide parameter range [16, 17].

We will consider initial pulses that are hyperbolic-secant shaped, so that $E(t) = A \text{sech}(t/\tau)$, where $\tau = 50 \text{ fs}$, and we choose A so that the initial pulse is a π pulse in the gain periods and a 2π pulse in the absorbing periods. We note that when $\tau = 50 \text{ fs}$, the full width half maximum (FWHM) duration is given by $[2 \ln(1 + \sqrt{2})] \tau \approx 1.763 \tau \approx 88 \text{ fs}$. We recall that the condition to be a π pulse in the gain medium is $(\mu_g/\hbar) \int_{-\infty}^{\infty} E(t) dt = \pi$, so that $A = 7.3 \times 10^6 \text{ V/m}$. We have previously shown that SIT modelocking is robust when the initial conditions are changed [16, 17].

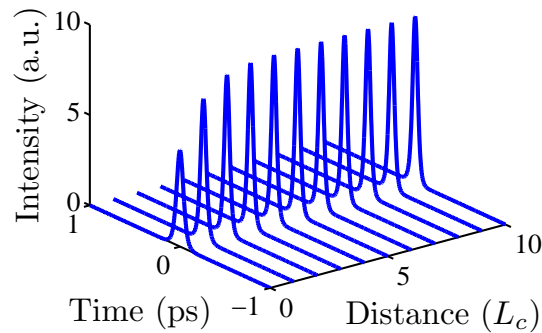


Fig. 2. Modelocked pulse evolution in presence of saturable loss. The saturable nonlinearity coefficient $\gamma = 10^{-12} \text{ m/V}^2$. We set $\bar{g} = 4$ and $\bar{a} = 5$. The dispersion coefficient (β_2) is set to zero.

3. Nonlinearity

3.1. Saturable loss ($\gamma > 0$)

The saturable nonlinearity coefficient γ is positive when the refractive index increases with intensity. Therefore, with $\gamma > 0$, the lateral optical mode becomes better confined in the core, and the loss saturates as the intensity of the pulse grows, as shown schematically in Fig. 1(a). We have found that the stable modelocked pulses are obtained when $\gamma < \gamma_c$, where γ_c is the critical value of the coefficient γ . In Fig. 2, we show an example of the evolution of an initial hyperbolic-secant pulse whose initial energy corresponds to a π pulse in the gain periods. Here, we have set $\gamma = 10^{-12} \text{ m/V}^2$. The gain normalized to the linear loss and the absorption normalized to the linear loss are set to 4 and 5, respectively. We see that the pulse reaches its stable equilibrium after propagating a distance that is only a few times the cavity length (L_c). The intensity of the initial pulse grows and the duration of the initial pulse narrows before the pulse equilibrates. In an SIT-modelocked laser, the pulse intensity and the pulse duration are determined by the values of the gain and absorption coefficients relative to the loss [15, 16]. However, in the presence of a saturable loss, pulses are further shaped by the intensity-dependent

loss in addition to the gain and absorption coefficients. A saturable loss favors more intense, shorter pulses. The additional pulse shaping depends on the magnitude of γ . In Fig. 3, we show the stable modelocked pulses with different values of γ . The maximum intensity of the pulse increases and the duration of the pulse decreases as γ increases. However, the laser becomes unstable when $\gamma > 1.9 \times 10^{-12} \text{ m/V}^2$ with $\bar{g} = 4$ and $\bar{a} = 5$.

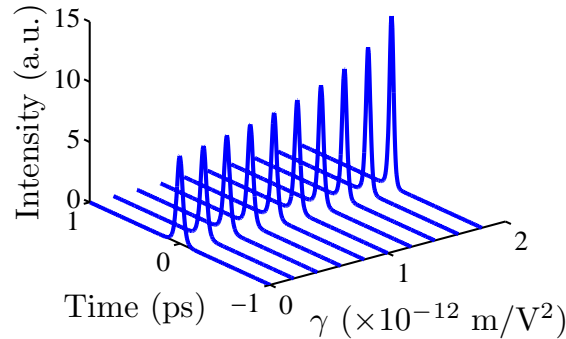


Fig. 3. Equilibrium modelocked pulse shapes vs. the saturable nonlinearity coefficient (γ). In each case, the pulse is shown after it has propagated a distance of $1000L_c$. We set $\bar{g} = 4$ and $\bar{a} = 5$. The dispersion coefficient (β_2) is set to zero.

In Fig. 4, we show the change in the normalized maximum intensity and in the duration of the stable modelocked pulses when γ changes. We define the duration as the full width at half maximum (FWHM) divided by $2\ln(1 + \sqrt{2}) = 1.763$. The maximum intensity of the pulses has been normalized by the maximum intensity of the pulse with $\gamma = 0$. The maximum intensity and the pulse durations have been calculated after the pulses have propagated a distance of $1000L_c$. In each case, the pulse becomes stable after propagating a distance of less than $100L_c$. We see that the maximum intensity of the pulse increases as γ increases. The maximum intensity of the pulse is larger by more than a factor of two when $\gamma = 1.9 \times 10^{-12} \text{ m/V}^2$ than it is when $\gamma = 0$. However, beyond this nonlinearity, i.e., $\gamma > 1.9 \times 10^{-12} \text{ m/V}^2$, the pulse becomes unstable. The pulse duration decreases as γ increases. We see that the stable pulse has a duration of ~ 43 fs when $\gamma = 0$, while the stable pulse has a duration of ~ 28 fs when $\gamma = 1.9 \times 10^{-12} \text{ m/V}^2$.

The critical value of γ , $\gamma = \gamma_c$, at which there is no stable pulse depends on the normalized gain and absorption coefficients. In Fig. 5, we present γ_c vs. \bar{a} for two values of \bar{g} . We find that the values of γ_c vary significantly when \bar{a} and \bar{g} change. As \bar{a} increases or \bar{g} decreases, we find that γ_c increases. By increasing \bar{a} and decreasing \bar{g} , the critical value of the saturable loss for stable operation can be significantly increased.

3.2. Saturable gain ($\gamma < 0$)

The saturable nonlinearity coefficient γ becomes negative when the refractive index of the core decreases as the light intensity increases. In this case, the overlap of the lateral mode with the core decreases, while the overlap with the lossy cladding increases as in Fig. 1(b). As a result, the gain will saturate as the light intensity increases. We show an example of the evolution of a stable modelocked pulse in Fig. 6 when saturable gain is present. As before, we choose an initial π pulse. In this case, the nonlinear coefficient γ is set to $-10 \times 10^{-12} \text{ m/V}$, and we use $\bar{g} = 4$ and $\bar{a} = 5$. We note that the intensity of the initial pulse decreases and the duration of

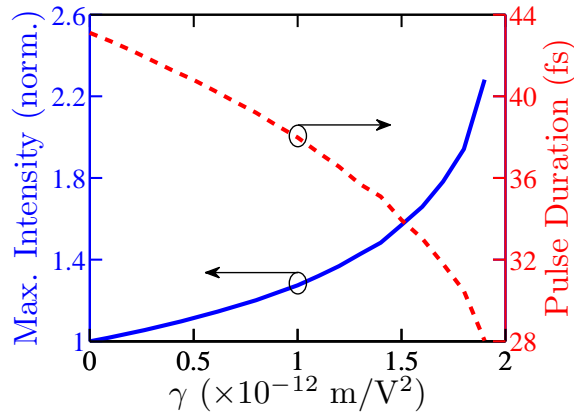


Fig. 4. The normalized maximum intensity and pulse duration (FWHM/1.763) of the stable modelocked pulse vs. the saturable nonlinearity coefficient (γ). We set $\bar{g} = 4$ and $\bar{a} = 5$. The dispersion coefficient (β_2) is set to zero.

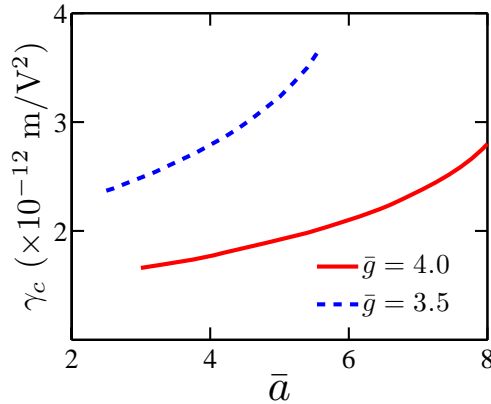


Fig. 5. The critical values of the saturable nonlinearity coefficient (γ_c) vs. the normalized absorption coefficient (\bar{a}) for two values of the normalized gain coefficient (\bar{g}). The dispersion coefficient (β_2) is set to zero.

the initial pulse increases before the pulse equilibrates. Similar to the case when the saturable loss is present, the pulse intensity and the pulse duration are determined by the saturable gain, in addition to the gain and absorption coefficients. In Fig. 7, we plot the stable modelocked pulses with different amounts of saturable gain. In each case, the pulse is shown after it has propagated a distance of $1000L_c$. Stable modelocked pulses become less intense and broader as γ becomes more negative. The pulses no longer equilibrate, but instead damp away when $\gamma \lesssim -68 \times 10^{-12} \text{ m/V}^2$.

In Fig. 8, we show the change in the normalized maximum intensity and in the duration (FWHM/1.763) of the stable modelocked pulses as $|\gamma|$ increases. The maximum intensity and the pulse duration values have been calculated after the pulses have propagated a distance of $1000L_c$. In each case, the pulse equilibrates after propagating a distance of less than $100L_c$. We see that the maximum intensity of the pulse at equilibrium decreases as $|\gamma|$ increases, i.e.,

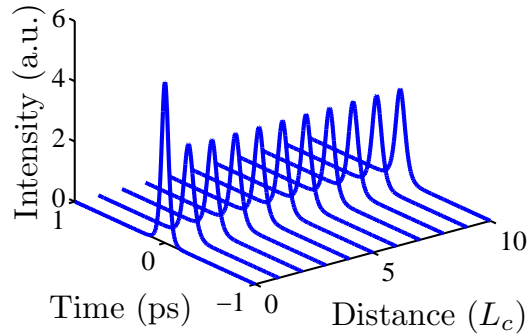


Fig. 6. Modelocked pulse evolution in the presence of saturable gain. The saturable nonlinearity coefficient $\gamma = -10 \times 10^{-12} \text{ m/V}^2$. We set $\bar{g} = 4$ and $\bar{a} = 5$. The dispersion coefficient (β_2) is set to zero.

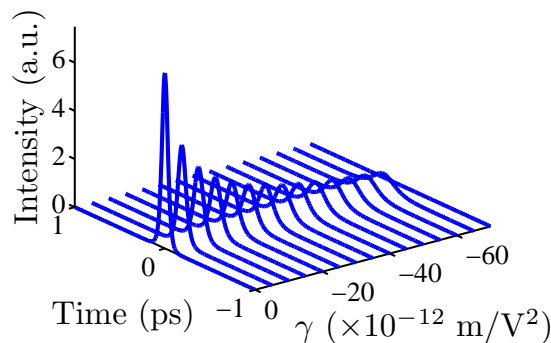


Fig. 7. Equilibrium modelocked pulse shapes vs. the saturable nonlinearity coefficient (γ). In each case, the pulse is shown after it has propagated a distance of $1000L_c$. We set $\bar{g} = 4$ and $\bar{a} = 5$. The dispersion coefficient (β_2) is set to zero.

when γ becomes more negative. The maximum intensity of the pulse is lower by approximately a factor of eight when $\gamma = -68 \times 10^{-12} \text{ m/V}^2$ than it is when $\gamma = 0$. When γ becomes more negative, pulses damp away. As $|\gamma|$ increases, the equilibrium pulse duration also increases. The stable pulse duration is 43 fs when $\gamma = 0$, while the stable pulse duration is 155 fs when $\gamma = -68 \times 10^{-12} \text{ m/V}^2$. We note that this value is more than 30 times larger in magnitude than the corresponding limit for saturable loss ($1.9 \times 10^{-12} \text{ m/V}^2$). Hence the constraint on the saturable gain is far less stringent than the constraint on the saturable loss.

In Fig. 9, we show the critical values of the saturable nonlinearity coefficient (γ_c) vs. the absorption coefficient (\bar{a}) for two values of the gain coefficient (\bar{g}) when the pulse experiences saturable gain during propagation. When $\gamma < \gamma_c$, the initial pulses do not equilibrate. The magnitude of γ_c is sharply peaked, first increasing rapidly as \bar{a} increases and then decreasing. On either side of the peak, $\bar{a}_{\text{peak}}(\bar{g})$, different physical mechanisms destabilize the initial pulse.

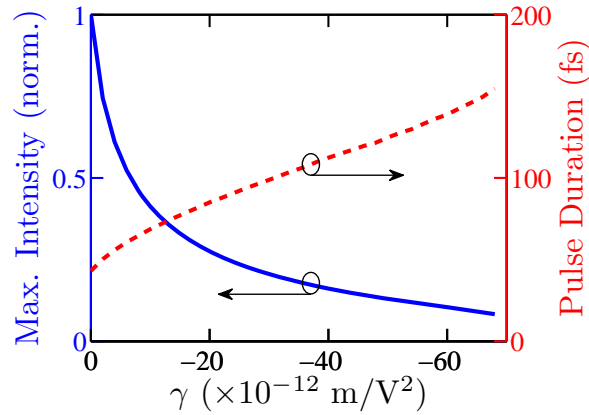


Fig. 8. The normalized equilibrium maximum intensity and pulse duration (FWHM/1.763) of the stable modelocked pulse vs. the saturable nonlinearity coefficient (γ). We set $\bar{g} = 4$ and $\bar{a} = 5$. The dispersion coefficient (β_2) is set to zero.

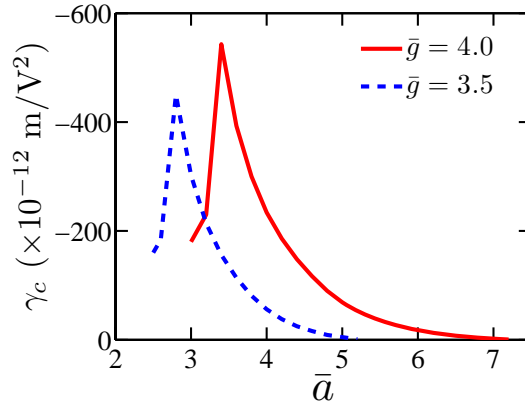


Fig. 9. Critical values of the saturable nonlinearity coefficient (γ_c) vs. the normalized absorption coefficient (\bar{a}) for two values of the normalized gain coefficient (\bar{g}). The dispersion coefficient (β_2) is set to zero.

When $\bar{a} < \bar{a}_{\text{peak}}$ and $|\gamma| > |\gamma_c|$, continuous waves grow and ultimately lead to the generation of multiple pulses. When $\bar{a} > \bar{a}_{\text{peak}}(\bar{g})$ and $|\gamma| > |\gamma_c|$, the initial pulse damps away.

4. Group velocity dispersion

In this section, we study the effects of the group velocity dispersion on SIT modelocking. We assume that the loss is linear and that it does not depend on the intensity of the light pulse, i.e., $\gamma = 0$. In Fig. 10, we show the evolution of a stable modelocked pulse in the presence of dispersion where the initial pulse is a π pulse. In this case, the dispersion coefficient $|\beta_2|$ is $5 \text{ ps}^2/\text{m}$. We use $\bar{g} = 4$ and $\bar{a} = 5$. We note that the solutions of Eq. (1) when $\beta_2 < 0$ are complex conjugates of the solutions when $\beta_2 > 0$ for equal values of $|\beta_2|$. Hence, the pulse intensity as a function of time is unaffected by the sign of β_2 . In Fig. 10, we see that the pulse's intensity decreases and its duration increases before the pulse equilibrates, but a modelocked

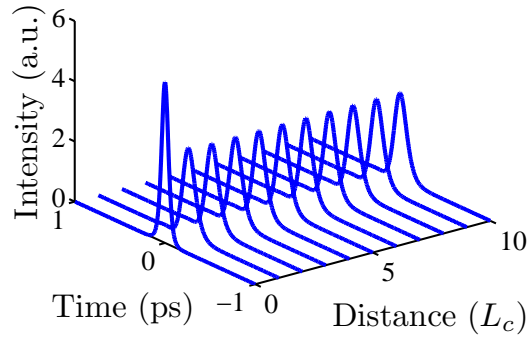


Fig. 10. Modelocked pulse evolution in presence of group velocity dispersion. The dispersion coefficient $|\beta_2| = 5 \text{ ps}^2/\text{m}$. We set $\bar{g} = 4$ and $\bar{a} = 5$. The saturable nonlinearity coefficient (γ) is set to zero.

solution exists. Pulse broadening increases as $|\beta_2|$ increases. In Fig. 11, we show the stable modelocked pulses in the presence of different amounts of dispersion. In each case, the pulse has propagated a distance of $1000L_c$. We note that the peak intensity of the stable modelocked pulse decreases and the duration increases as $|\beta_2|$ increases. There is no modelocked solution when $|\beta_2| > 82 \text{ ps}^2/\text{m}$. Beyond this critical value of dispersion, the initial pulse damps away.

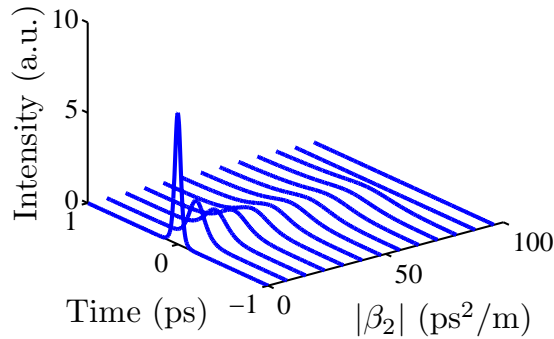


Fig. 11. Equilibrium modelocked pulse shapes vs. group velocity dispersion coefficient ($|\beta_2|$). In each case, the pulse is shown at a propagation length of $1000L_c$. We set $\bar{g} = 4$ and $\bar{a} = 5$. The saturable nonlinearity coefficient (γ) is set to zero.

In Fig. 12, we draw the change in the normalized maximum intensity and in the duration (FWHM/1.763) of the stable pulses as the group velocity dispersion is varied. The maximum intensity has been normalized by the maximum intensity of the pulse with $|\beta_2| = 0$. The maximum intensity and the duration have been calculated after the pulses have propagated a distance of $1000L_c$. In each case, the pulse becomes stable after propagating a distance of less than $100L_c$. We see that the maximum intensity of the pulse decreases as $|\beta_2|$ increases. The maximum intensity of the pulse decreases by approximately a factor of 10 when $|\beta_2| = 80 \text{ ps}^2/\text{m}$

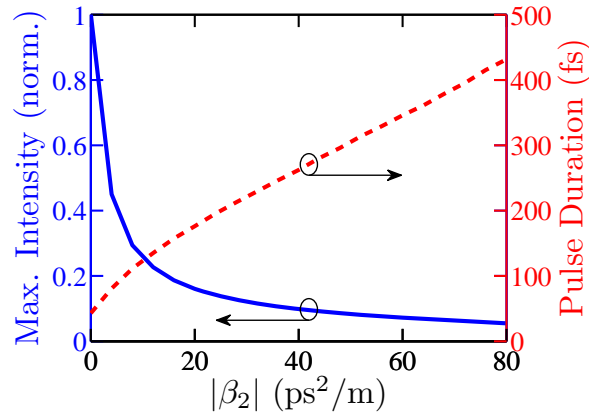


Fig. 12. The normalized maximum intensity and pulse duration (FWHM/1.763) at equilibrium vs. the dispersion coefficient (β_2). We set $\bar{g} = 4$, $\bar{a} = 5$. The saturable nonlinearity coefficient (γ) is set to zero.

compared to when $|\beta_2| = 0$. The equilibrium pulse duration when $|\beta_2| = 0$ is 43 fs, while the equilibrium pulse duration is 432 fs when $|\beta_2| = 80 \text{ ps}^2/\text{m}$.

The critical values of the dispersion coefficients for stable modelocking $|\beta_{2c}|$ have been plotted in Fig. 13 vs. \bar{a} for two different values of \bar{g} . We see that the critical value first increases as \bar{a} increases up to $\bar{a}_{\text{peak}}(\bar{g})$, and then decreases. The equilibrium pulse duration is always larger when dispersion is present than when it is not. Analogous to the case shown in Fig. 8, we find that when $\bar{a} < \bar{a}_{\text{peak}}(\bar{g})$ and $|\beta_2| > |\beta_{2c}|$, multiple pulses are generated, and when $\bar{a} > \bar{a}_{\text{peak}}(\bar{g})$ and $|\beta_2| > |\beta_{2c}|$, the initial pulse damps away.

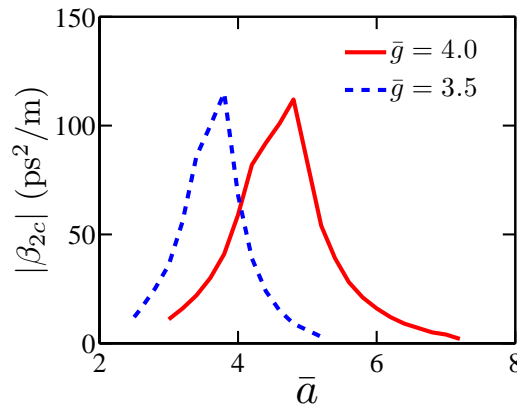


Fig. 13. The critical values of the dispersion coefficient ($|\beta_{2c}|$) vs. the normalized absorption coefficient (\bar{a}) for two values of the normalized gain coefficient (\bar{g}). The saturable nonlinearity coefficient (γ) is set to zero.

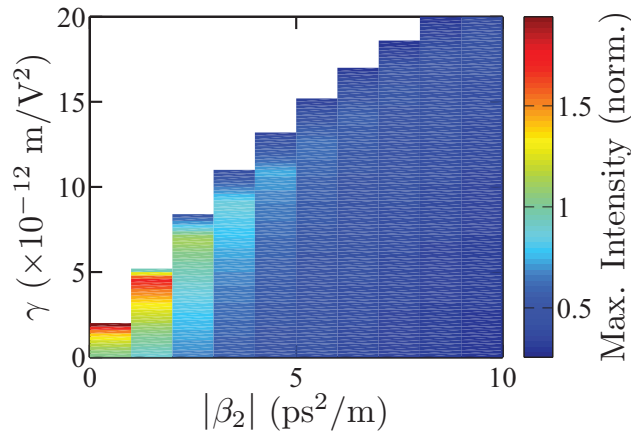


Fig. 14. Contour plot of the normalized maximum intensity vs. the saturable nonlinearity coefficient ($\gamma > 0$) and group velocity dispersion coefficient (β_2). The maximum intensity has been calculated after the pulse has propagated a distance of $1000L_c$. We set $\bar{g} = 4$ and $\bar{a} = 5$.

5. Saturable nonlinearity and group velocity dispersion

In this section, we will discuss the realistic case in which a saturable nonlinearity and group velocity dispersion are simultaneously present. We note once more that the solutions when $\beta_2 < 0$ are the complex conjugates of those when $\beta_2 > 0$ and $|\beta_2|$ is unchanged. In Fig. 14, we present a contour plot of the maximum intensity of the equilibrium modelocked pulses as the saturable loss and group velocity dispersion vary. The unstable region is shown blank. The maximum intensity has been normalized by the value of the maximum intensity of the stable modelocked pulse with $\gamma = 0$ and $\beta_2 = 0$. We note that the critical value of the saturable loss increases significantly when $|\beta_2|$ increases. We also note that the maximum intensity varies significantly with the change of the saturable loss when $|\beta_2| < 4 \text{ ps}^2/\text{m}$. The maximum intensity decreases as $|\beta_2|$ increases for a fixed value of γ . When $|\beta_2| > 4 \text{ ps}^2/\text{m}$, the maximum intensity does not vary much as γ changes, and the normalized maximum intensity is less than 1 even when $\gamma \approx \gamma_c$. The critical value of dispersion coefficient $|\beta_{2c}|$ increases as γ increases. We show a contour plot for the duration of the modelocked pulse when saturable loss and dispersion are varied in Fig. 15. We note that the duration of the modelocked pulse increases when $|\beta_2|$ increases for any value of γ . However, the duration of the modelocked pulse remains approximately the same when γ increases for a fixed value of $|\beta_2|$. When dispersion is present, a larger saturable loss can be tolerated. Conversely, when saturable loss is present, pulse broadening due to dispersion is diminished. The limits on saturable loss and chromatic dispersion become less stringent when the other is present.

In Fig. 16, we show a contour plot for the maximum intensity of the stable modelocked pulses when saturable gain and group velocity dispersion are simultaneously present. We note that the maximum intensity only changes significantly as $|\beta_2|$ and γ change when $|\beta_2| \lesssim 5 \text{ ps}^2/\text{m}$ and $\gamma \gtrsim -20 \times 10^{-12} \text{ m/V}^2$. When $\gamma \lesssim -20 \times 10^{-12} \text{ m/V}^2$, the maximum pulse intensity of the modelocked pulse changes very little as $|\beta_2|$ changes. Similarly, when $|\beta_2| \gtrsim 5 \text{ ps}^2/\text{m}$, the maximum intensity of the modelocked pulse is essentially same for any amount of saturable gain. Critical values of the saturable gain do not vary much when the dispersion coefficient is

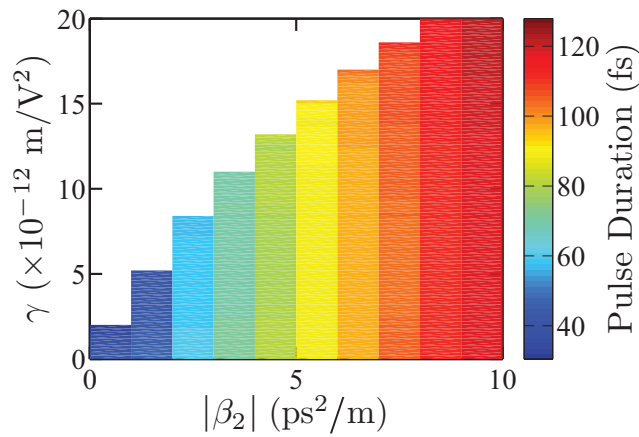


Fig. 15. Contour plot of the duration vs. the saturable nonlinearity coefficient ($\gamma > 0$) and group velocity dispersion coefficient (β_2). The duration has been calculated after the pulse has propagated a distance of $1000L_c$. We set $\bar{g} = 4$ and $\bar{a} = 5$.

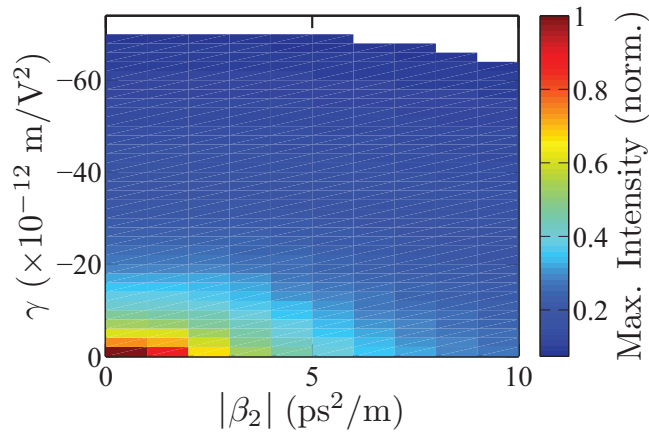


Fig. 16. Contour plot of the normalized maximum intensity vs. the saturable nonlinearity coefficient ($\gamma < 0$) and group velocity dispersion coefficient (β_2). The maximum intensity has been calculated after the pulse has propagated a distance of $1000L_c$. We set $\bar{g} = 4$ and $\bar{a} = 5$.

varied. The critical value of dispersion coefficient $|\beta_{2c}|$ decreases as $|\gamma|$ increases. In Fig. 17, we show a contour plot of the stable modelocked pulse duration when both saturable gain and dispersion vary. We note that the pulse duration increases when the saturable gain increases for any $|\beta_2|$. Similarly, the pulse duration increases when $|\beta_2|$ increases for any amount of saturable gain. The equilibrium duration decreases by well over a factor of 100 before the initial pulse becomes unstable. However, the equilibrium pulse duration when the saturable gain is just below the critical value stays approximately the same as $|\beta_2|$ is varied.

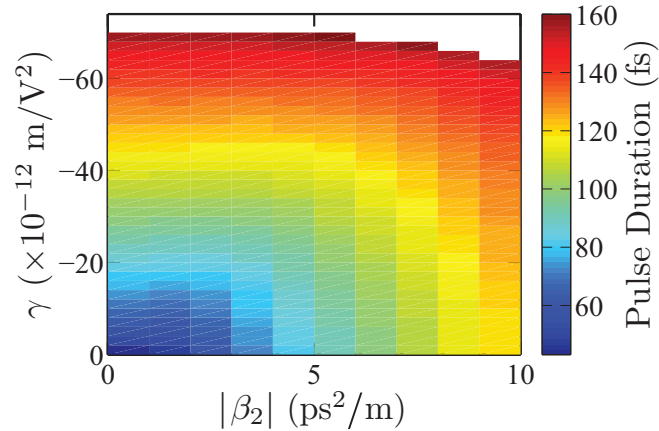


Fig. 17. Contour plot of the duration vs. the saturable nonlinearity coefficient ($\gamma < 0$) and group velocity dispersion (β_2). The duration has been calculated after the pulse has propagated a distance of $1000L_c$. We set $\bar{g} = 4$ and $\bar{a} = 5$.

6. Conclusion

In conclusion, we show that QCLs can be modelocked using the SIT effect in the presence of a saturable nonlinearity, either saturable loss or saturable gain, and in the presence of group velocity dispersion, as long as their magnitudes are below critical limits. However, the modelocked pulse's equilibrium duration and maximum intensity are affected. The saturable loss sets a more stringent limit on $|\gamma_c|$ than does the saturable gain. The limits are $1.9 \times 10^{-12} \text{ m/V}^2$ and $68 \times 10^{-12} \text{ m/V}^2$ with $\bar{g} = 4$ and $\bar{a} = 5$, which differ by more than a factor of 30. However, when group velocity dispersion is present, the limit on $|\gamma_c|$ increases significantly in the case of saturable loss, while $|\gamma_c|$ is relatively unaffected in the case of saturable gain. The critical limits of saturable nonlinearity and group velocity dispersion also change significantly when \bar{g} and \bar{a} change.

The saturable nonlinearity calculated by Gordon *et al.* ($\sim 10^{-11} \text{ m/V}^2$) [19] and the group velocity dispersion calculated by Choi *et al.* ($-4.6 \text{ ps}^2/\text{m}$) [20] for particular QCLs are within the stable regime in Fig. 14 and in Fig. 15. The magnitude of the saturable nonlinearity coefficient γ depends on the gain linewidth and on the lateral dimension of the laser core. Thus, one can always reduce γ in principle to ensure stable operation by properly designing the QCL.